PREPARATION OF CRYSTALLINITY TAILORED SILK FIBROIN-SODIUM ALGINATE BASED FLOATING MICROBEADS FOR NEVIRAPINE DELIVERY

BHUPESH DIGAMBAR PATIL[#], SOPAN NAMDEV NANGARE[#] and LAXMIKANT RAMVALLABH ZAWAR[*]

Department of Pharmaceutics, H. R. Patel Institute of Pharmaceutical Education and Research, Shirpur Dist.: Dhule 425405, Maharashtra State, India
✉ *Corresponding author: L. R. Zawar, shwet.zawar@gmail.com*
[#]*These authors contributed equally to this work*

Received April 13, 2023

The present work anticipated crystallinity-tuned silk fibroin (SFIB)-sodium alginate floating microbeads (MB) as a candidate for nevirapine (NEV) sustained release. Briefly, crystallinity tuning was accomplished using solvent annealing. The changes in structural conformation of SFIB were validated using FTIR spectroscopy. Here, the tangent baseline method revealed changes in crystallinity of floating NEV-loaded SFIB-MB. Importantly, solvent annealing offers conversion of amorphous 'α-helix' to crystalline 'β-sheet' of SFIB, helping to modify drug release from the matrix of SFIB-sodium alginate. As well, NEV-loaded SFIB-MB demonstrated good floating profile. The NEV-loaded SFIB-MB with ethanol (ETH-6) annealing for 6 hours shows 25.853% drug release at 12 hours (pH = 1.2), compared to untreated NEV-loaded SFIB-MB (65.132%, 12 hours, log $p < 0.0001$). The release kinetics of batch ETH-6 revealed first-order release kinetics and Fickian diffusion ($n = 0.468$) was found to be the drug diffusion mechanism. Therefore, crystallinity-modified floating NEV-loaded SFIB-based MB will open a new door for modified drug delivery.

Keywords: silk fibroin, nevirapine, floating drug delivery, microbeads, crystallinity modulation, solvent annealing

INTRODUCTION

Since its inception, oral dosing has been the most common route for administration of a therapeutically active agent. It is crystal clear that the goal of oral dose formulation is to achieve drug absorption through the gastrointestinal tract (GIT). However, quick gastrointestinal movement may result in the partial release of the active agent to the targeted area. Hence, due to the rapid gastric emptying issue, it is difficult to retain the dosage from the stomach site, resulting in reduced dosage potency.[1] In light of current discoveries, modified oral dosage forms can effectively enable tailored drug incorporation.[2] Efforts are taken to establish a novel drug delivery system that can maintain active concentration in plasma within therapeutic ranges for extended periods. Moreover, it helps to diminish variability in plasma drug concentration at a fixed state by distributing the drug in a regulated and repeatable way.[3] Out of several types of dosage forms, researchers are particularly interested in the gastro retentive drug delivery system (GRDDS) for a specific drug that acts regionally and has absorption openings in the upper GIT.[4,5] For that purpose, swelling and expansion-mediated systems, floating systems, bio(muco)adhesive dosage forms, *etc*. have been developed. Principally, it has been achieved using different types of excipients selected based on the density of the material, shape, and size. Also, their adhesive behavior and swelling index (SI) need to be considered for intended pharmaceutical formulations.[6] Particularly, in GRDDS, researchers have been focused on floating drug delivery systems (FDDS). It is due to their simple process and high effectiveness in formulation development.[7,8] Moreover, it has been reported that the FDDS can extend the duration a dosage form spends in the stomach, hence increasing the drug's oral bioavailability.[9,10] The use of effervescent agents produces carbon dioxide gas that can result in disturbances in the microbial

environment of the GIT.[11] For FDDS, a lower-density natural polymeric substance, compared to the stomach fluid density, provides superior buoyant properties.[12] In this case, the maximum gastric retention period that does not allow worsening of the drug exists at the absorption site only.[13,14] Presently, floating dosage forms, mainly floating microbeads (MB), have attracted major interest for drug delivery. To date, different active agents have been reported in MB-based drug delivery systems, including metronidazole,[15] cefuroxime axetile,[16] sumatriptan,[17] loratadine,[18] metformin,[19] clarithromycin,[20] ciprofloxacin HCl,[21] *etc*. All herein cited studies assured that the use of MB could offer the potential of an extended gastric retention period, uniform distribution via GIT, minimized hazard of local inflammation, adjustable release, maximum drug absorption from the stomach, *etc*. For the design of floating MB, the use of low-density polymeric materials is revealing a new alternative. Recently, different proteins have also been divulged for pharmaceutical applications that can be effectively preferred in the design of MB. Despite this, modification of drug release from advanced MB is a critical challenge for the scientific community.

Silk fibroin (SFIB) is a major industrial waste protein present in silk cocoons. In the last decades, it has been widely used for several biomedical applications. As per data, it has been used for the development of floating electrospun nanofibers,[11] microspheres,[12] *etc*. It has been preferred for the delivery of absorption window-specific and poorly soluble drugs, such as felodipine, lafutidine, *etc*. As a result, we choose SFIB as a polymer for the proposed work.[22] A literature survey reported that SFIB is biocompatible and decomposable.[23] Notably, it has a low density, as compared to stomach juices, indicating that it is suitable for the construction of floating dosage forms also.[12,24] Overall, owing to its special qualities, such as low density, biocompatibility, biodegradability, *etc*., SFIB microspheres have previously been observed for regulated drug delivery and as enzyme vehicles.[25] In addition, SFIB presents sufficient flexibility, good strength, ease of chemical modification, *etc*.[26] As a result, SFIB can be used as a major substitute for creating dosage forms.

In terms of SFIB biochemistry, SFIB is divided into two states: an amorphous form known as silk I due to its 'α-helices' structure and a crystal-like form known as silk II due to its high 'β-sheet' concentration. The physicochemical features of SFIB, like tensile strength, water solubility, and biodegradability, are all tuned by the β-sheets conformation. Interestingly, the transformation of SFIB from an 'α-helix' to a 'β-sheet' configuration can be aided by the use of organic solvent annealing.[27] Surprisingly, there are no published studies on crystallinity-regulated floating MB for modified drug release applications. As a result, we aimed to utilize a low-density SFIB to compose crystallinity-modified floating MB. The *in-vitro* degradation investigation on SFIB fibrous scaffolds found that scaffolds with increased crystallization degraded more slowly in SFIB. As a result, SFIB's crystallinity modification capabilities activate scaffold degradation to be regulated, resulting in longer and controlled delivery of active components.[28] According to a survey of the literature, sodium alginate is often used to achieve long-term active distribution.[29,30] because it attacks the mucosa of the stomach,[31,32] and can improve the active bioavailability.[33] In this, calcium ions assist to produce a persistent and biocompatible gel.[34] The combination of SFIB and sodium alginate will guide to added merits in floating MB, compared to the traditional approach.

In the present study, nevirapine (NEV) is preferred as a model drug. It is a human immune-deficiency virus type I non-nucleoside reverse transcriptase inhibitor. It is poorly soluble in water (belongs to BCS class II).[35] Besides, NEV is effectively absorbed orally in humans. As per data, NEV is a good candidate for floating medication delivery systems, since it is highly soluble and absorbed at pH < 3.[36] From the jejunum to the descending colon, as well as from the upper to lower portions of the gastrointestinal tract, the NEV absorption rate decreased.[37] Therefore, a floating oral delivery of NEV is anticipated to retain the NEV at the absorption site only, which can assist in improving absorption and bioavailability.

The anticipated work reported the conversion of the 'α-helix' to 'β-sheet' approach for crystallinity modification of NEV-loaded SFIB-IPN-based floating MB followed via the solvent annealing method. As far as we are aware, there is no research study on crystallinity adaptation for floating MB. In this work, industrial silk cocoons waste materials were preferred for the development of floating MB. Spectroscopic characterizations were performed to assure the

synthesis of NEV-loaded SFIB-based floating MB. Finally, the NEV-loaded SFIB-based floating MB was further evaluated for floating profile and release kinetics analysis. The use of solvent treatment resulted in the conversion of 'α-helix' to 'β-sheet', which affected the release profile of NEV, compared to the case of the non-treated MB. It is expected that crystallinity-tuned floating MB will release a new vista for pharmaceutical drug delivery applications.

EXPERIMENTAL

Materials

Nevirapine (NEV) was obtained as a gift sample from Cipla Ltd. Goa, India. Sodium carbonate (anhydrous, 99.50%) was purchased from Rankem Laboratory Reagent, Thane, Maharashtra. Lithium bromide (anhydrous, 98%) and sodium alginate (low viscosity, 216.12 g/mol) were obtained from Loba Chemie Pvt. Ltd. Mumbai. Calcium chloride (dihydrate) was procured from Merck Life Science Private Limited, Mumbai. Di-ionized water (DDW) was prepared in the research laboratory. Acetone (99.80%) and isopropyl alcohol (99.00%) were purchased from Rankem Laboratory Reagent, Thane, Maharashtra. Ethanol (99.50%) and methanol (99.00%) were purchased from Anil Cottage Industries, Wardha, Maharashtra. Dialysis membrane-110 was procured from Himedia Lab. Pvt. Ltd. Mumbai (molecular weight cut-off 7000 Da). Silk cocoons were provided by Sanjivani Reshim Udyog Samuh (collection center), Igatpuri, Nashik.

Methods

Extraction of silk fibroin (SFIB)

In this step, SFIB was isolated from silk cocoons obtained from Sanjivani Rreshim Udyog Samuh, a reeling house (collection center). Isolation of SFIB was accomplished using a formerly reported method. In brief, at first, a research laboratory hot air oven was used to dry the collected silkworm cocoons. After that, the dried silk cocoons were checked for trapped foreign items and then the cocoons were chopped into little pieces (approximately 5 mm to 1 cm). Then, alkali degumming was performed to separate the sericin (second hydrophilic yellow-colored protein). For this, the cut pieces were firstly immersed in a freshly prepared 0.5% sodium carbonate that was subjected to boiling at 80 °C for 40 minutes, with constant stirring with a glass rod. In this step, the glue-like yellow color sericin containing sodium carbonate was separated from the solid mass.[38] Following this, the entire mass was rinsed with distilled water several times until clear water was recovered. Thus, it was ensured that the obtained white material was completely free of sericin. Complete drying of mass was performed at 60 °C using a laboratory vacuum oven. In the second step, the cleaned silk threads (10 g) were liquefied in 40 mL of 9.3 M LiBr solution at 60 °C for 4 hours. After that, obtained SFIB liquid was subjected to the removal of LiBr using a dialysis membrane against distilled water for two days at room temperature (RT) with continuous stirring at 400 rpm. In this step, process water was changed every 6 h, providing the solvent for the removal of LiBr at a high rate. Finally, the SFIB solution was cold centrifuged for 20 minutes at 15 °C (12000 rpm), which provided a pure SFIB supernatant, whereas foreign and undissolved matter settled down at the bottom of the centrifuge tube.[39] For confirmation of the isolation of SFIB from silk cocoons, different tests were performed, including melting point, ultraviolet-visible (UV-Vis) spectroscopy, and the laboratory protein test.

Preparation of self-floating NEV-loaded SFIB-IPN-MB

The process for the design of floating MB was achieved using the following formulations (Table 1). Herein, NA_1, NB_1 and NC_1 were preferred for the optimization of self-floating NEV-loaded SFIB-IPN-MB. In brief, 200 mg of NC_1 was dissolved in 10 mL of methanol by sonication for 30 minutes in a bath. After that, this solution was dispersed in freshly prepared 12.5 mL of NB_1 in concentrations of 4% (w/v), 6% (w/v), and 8% (w/v), separately. Then, it was incorporated into the NA_1 with different concentrations, such as 3% (w/v), 4% (w/v), and 6% (w/v).

Table 1
Formulations of self-floating NEV-loaded SFIB-IPN-MB

Sr. No.	Formulation factors		
	NA_1	NB_1	NC_1
B_1	4% (w/v)	6% (w/v)	-
B_2	3% (w/v)	4% (w/v)	-
B_3	3% (w/v)	4% (w/v)	200 mg
B_4	4% (w/v)	6% (w/v)	200 mg
B_5	6% (w/v)	8% (w/v)	200 mg

NA_1: % of SFIB (w/v); NB_1: % of sodium alginate (w/v); NC_1: Drug (mg) in 10 mL methanol

The subsequent solution was then injected into 200 mL of $CaCl_2$ solution [10% (w/v)], using a 25 gauge (0.8 × 30 mm) syringe needle at a 45° angle. Finally, to strengthen the mechanical strength of the MB, they were left in the same solution for 2 hours at 25 °C. Following that, the MB was rinsed in deionized water and dried at room temperature (RT). Using the same process, batches B_1 and B_2 were prepared as plain floating MB, without the addition of NEV.[40]

Process of solvent treatment by different solvents

In this step, the above-prepared NEV-loaded SFIB-IPN-MB was annealed with three different solvents, namely ethanol (ETH), isopropyl alcohol (IPA), and acetone (ACT). Initially, 50 mL of ETH was poured into a separate 1000 mL clean glass beaker, whereas another 250 mL beaker was placed inside it to helps place the Petri plate of NEV-loaded SFIB-IPN-MB. In the case of the first sample of optimized NEV-loaded SFIB-IPN-MB, 2 g of NEV-loaded SFIB-MB was weighed and added to the Petri plate. Afterward, Petri plates were kept in the above-prepared ETH-containing beaker for solvent annealing treatment, wherein the beaker was airtight with the help of aluminum foil to avoid the leakage vapor of ETH. Finally, a sample was allowed for 2, 4, and 6 hours at a programmed value of 45 °C in a laboratory oven.[38] The same procedure was preferred for other solvents, namely IPA and ACT. The changes in crystallinity were performed using the previously reported method. In brief, the tangent baseline approach was utilized to calculate the degree of crystallinity of NEV-loaded SFIB-IPN-MB using the same recorded FTIR spectra.[27,41]

In short, for crystallinity estimates, the intensity of two consecutive peaks for SFIB composed of 'amide I' and 'amide II' was taken into account. At first, the tangent was drawn from the peak of 'amide I' to the peak of 'amide II'. The intensity of the peaks was then quantified in terms of height by drawing a perpendicular line from the tip of a peak to the midway of the tangent (cm). Finally, the degree of crystallinity was determined using the formula below (1):

$$\text{Degree of crystallinity} = \frac{a}{b} \quad (1)$$

where a/b is the ratio of amide I peak intensity to amide II peak in cm^{-1}.[38]

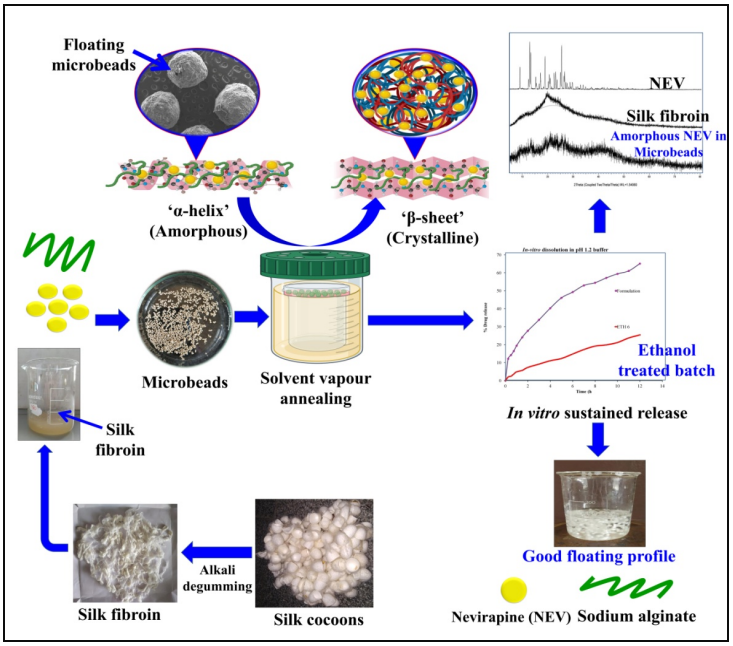

Scheme 1: Preparation procedure followed in this work

Spectroscopic and *in-vitro* characterizations

Spectroscopic characterization

Fourier transform infrared (FTIR) spectroscopy

The ATR-FTIR analysis of dry powders of SFIB, NVP, sodium alginate, physical mixture, plain SFIB-MB, NEV-loaded SFIB-MB, and solvent-treated NEV-loaded SFIB-IPN-MB was performed using an FTIR spectrophotometer (Shimadzu IRAffinity-1S). In brief, 2 mg of material was taken and carefully crushed with KBr in a mortar using a pestle for proper mixing. After that, the standardized sample was positioned in a sample container, and the bands were recorded for analysis in the wavenumber range from 400 cm^{-1} to 4000 cm^{-1}.[42]

Differential scanning calorimetry (DSC)

Herein, a DSC (DSC 60 plus-Shimadzu, Japan), fitted with an intra-cooler and chilled cooling system, was used to examine the thermal characteristics of dry powders SFIB, NVP, and NEV-loaded SFIB-IPN-MB.[43] In brief, the thermogram of each sample was achieved by scanning over a thermal range of 25-350

°C, followed by fast cooling in DSC analysis. In this case, the standard reference was an empty aluminum pan.

Powder X-ray diffraction studies (PXRD)

The PXRD patterns of lyophilized powders of SFIB, NVP, and NEV-loaded SFIB-IPN-MB were recorded at RT using an XRD (Bruker D2 Phase, Germany) with Cu kα radiation (1.54 Å), at 40 kV and 40 mA. The diffractometer had a two-slit compensating slit, and silicon pellets were used to calibrate the precision of the peak positions. The samples were then subjected to continuous XRD examination throughout an angle range of 3-40° as a 2θ with a phase size of 0.01 and a step period of 1 second. During the analysis, the sample holder spun in an equivalent plane at a speed of 30 rpm.[38]

Scanning electron microscopy (SEM)

In brief, a Jeol 6390LV SEM (USA) was used to observe the external morphology of a NEV-loaded SFIB-IPN-MB. Double-adhesive tape was applied to an aluminum stub for sample preparation and then it was detached to disclose an adhesive-coated aluminum stub. The stubs were then covered with gold to a width of 300 microns in an argon atmosphere with a high vacuum evaporator. The covered stub was then subjected to a 15 kV accelerating voltage for 90 seconds under 0.1 torr argon compression. SEM images of NEV-loaded SFIB-IPN-MB were captured from various angles at various magnifications.[12]

Percentage entrapment efficiency (% EE) and drug content

In this step, 50 mg of NEV-loaded SFIB-IPN-MB was preferred to calculate percentage entrapment efficiency. Initially, the MB was crushed using a pestle and mixed with 10 mL of 0.1 N HCl. Then, the mixture was bath sonicated for 1 hour at 37 °C and then subjected to filtration. Finally, the absorbance was examined at 314 nm against a blank of 0.1 N HCl buffer.[38] The concentration of NEV was calculated using a slope of a calibration curve that was performed in the same buffer (pH = 1.2). The same experiment was performed in triplicate to confirm the uniformity of EE (%) in the formulated NEV-loaded SFIB-IPN-IPN-MB. For calculation of the drug content, 50 mg of NEV equivalent of NEV-loaded SFIB-IPN-MB was taken into 100 mL of 0.1 N HCl buffer. This solution was bath sonicated for 2 hours to dissolve the NEV from MB. Finally, the absorbance was observed at 314 nm against a blank (0.1 N HCl buffer) and the percentage drug content was measured in NEV-loaded SFIB-IPN-MB (in triplicate).[44]

Micromeritic properties

Bulk density and tapped density

Bulk density is the ratio between the mass of the material and the volume occupied by the material. Herein, a fixed amount of each batch of floating SFIB-MB was subjected to weight measurement and volume measurement (in triplicate). After that, the bulk density was reported by the formerly documented method:[12]

$$\text{Bulk Density (BD)} = \frac{S_1}{S_2} \quad (2)$$

where S_1 = mass of MB and S_2 = volume acquired by MB.

In the case of the tapped density of floating SFIB-MB, fixed amounts of each batch of floating SFIB-MBs were subjected to weight measurement. After that, floating SFIB-MBs were transferred to the measuring cylinder, where they were gently tapped 20 times using a laboratory-tapped density apparatus. As a response, the volume of the sample was noted as tapped volume. The same procedure was performed for each batch in triplicate. The tapped density was determined by the following formula:[12]

$$\text{Tapped Density (TD)} = \frac{M_1}{M_2} \quad (3)$$

where M_1 = mass of MB and M_2 = tapped volume.

Angle of repose and Carr's compressibility index

The angle of repose was used to determine the flowability of floating SFIB-MB (B_1– B_5). In brief, the fixed funnel free-standing cone process was employed to verify the angle of repose of floating SFIB-MB of each batch in triplicate. For 10 g of floating SFIB-MB, the angle of repose was measured using the previously documented formula:[12]

$$\text{Tan } \theta = \frac{h}{r} \quad (4)$$

where θ = angle of repose, h = height of the pile, and r = radius of the pile.

In the case of Carr's compressibility index, the previously calculated tapped density and bulk density were preferred. The well-documented formula was used to report the flowability of floating SFIB-MB:[45]

$$\text{Carr's compressibility index (\%)} = \frac{TD-BD}{TD} \text{ x } 100 \quad (5)$$

Particle size analysis

In this step, the particle size of floating SFIB-MB was determined using a Nanoplus 3 (Particulate System Micromeritics, USA). In brief, 5 mL of freshly prepared floating SFIB-MB samples were checked for particle size measurement at 25 °C. The same experiment was performed in triplicate to assured the average diameter of floating SFIB-MB.

Floating profile of SFIB-MB

Herein, 500 mg of floating SFIB-MBs were accurately weighed and poured into a 250 mL beaker containing 150 mL of pH = 1.2 HCl buffer. The time needed for SFIB-MB to float on the superficial pH 1.2 HCl buffer was measured as floating lag time (FLT).[38] For calculation of percent buoyancy, 500 mg of SFIB-MB were accurately weighed and transferred in a 250

mL beaker holding 150 mL of HCl buffer (pH = 1.2). Then, the number of SFIB-MB that floated about the total amount of MB put into the beaker was calculated as percent buoyancy. The reported formula was used to compute percent buoyancy:[38]

$$\text{Percent buoyancy of MB} = \frac{P_1}{P_2} \times 100 \quad (6)$$

where P_1 = total amount of MB floated (mg) and P_2= total amount of MB added (mg).

Total floating time (TFT) was documented using a USP dissolution apparatus type II. Herein, 500 mg of SFIB-MB was poured into 900 mL of dissolution media (HCl buffer, pH =1.2) at 37 ± 0.5 °C with constant stirring at 50 rpm. Herein, TFT was calculated based on the duration required to float SFIB-MB on the surface of the vessel's dissolution media.[38]

In-vitro *dissolution study*

In-vitro dissolution of SFIB-MB was performed using a USP dissolution apparatus-I, using 40 mg of NEV equivalent SFIB-MB placed into a rotating basket. Dissolution was performed in 900 mL of 0.1 N HCl buffer (pH = 1.2). Importantly, throughout the dissolution investigation, processing variables, such as temperature (37 ± 0.5 °C) and basket spin speed (50 rpm) were kept constant. To maintain sink condition, 5 mL of dissolving medium was withdrawn at each sampling time point and replaced with the same quantity of fresh buffer solution. Whatman filter paper (25 mm, Whatman Inc., USA) was used to filter the withdrawn testing sample. Then, a UV-Vis spectrum was recorded at 314 nm, and the percent drug release was computed. The same experiment was performed for each solvent-treated SFIB-MB.

After that, the impact of modification in percent drug release from SFIB-MB was documented using the release kinetics models compared to the optimized non-treated SFIB-MB. For calculated release kinetics and other statistical values, PCP-Disso-v3 software was utilized. For an explanation of the drug release mechanism, mostly three release components were calculated, including 'n', which represents the release exponent, 'k' – the release rate constant, and 'r^2' – the regression factor. Based on this factor, the best-fit model was confirmed, along with the percent release and drug transport mechanism recorded.[46] In brief, different release kinetics models, such as zero order, first order, Higuchi matrix, Korsmeyer Peppas, and Hixon Crowell, were tested. In brief, zero-order release kinetics was calculated using cumulative percent drug release vs time, whereas first-order release kinetics was assured using the log of percent cumulative drug release vs time. Also, the Korsmeyer Peppas model was validated using the log of percent cumulative drug release vs log time, whereas the Higuchi model was verified using the percent cumulative drug release vs square root of time. Finally, the Hixon Crowell release kinetics was verified using the cube root of percent cumulative drug release vs time. Based on the statistical data, the best-fit release kinetic model was calculated for the optimized formulation.

Statistical and model-independent method

As a statistical approach, the paired 't'-test was utilized to compare the dissolution profiles of the formulation batch and ETH-6. Furthermore, the difference factor (f_1) and similarity factor (f_2) were determined to ensure that the dissolution profile of non-treated beads and ETH-6 beads was consistent.

RESULTS AND DISCUSSION

In this study, the isolation of SFIB from silk cocoons provided almost 75-80% practical yield. After that, the degradation point of SFIB was observed to be 256-272 °C. It shows the UV absorption band (λ max) at 276 nm wavelength. Overall, preliminary testing assured the isolation of SFIB from silk waste cocoons. After that, based on different concentrations of each component, such as concentration of SFIB, sodium alginate and drug, floating SFIB-MBs were prepared using a simple method. Interestingly, the designed SFIB-MB shows a spherical shape and smooth surface morphology. Herein, electrostatic forces between SFIB-sodium alginate and the lowest viscosity of the dispersion were found to be important factors for the design of SFIB-MB. Based on initial trials, certain concentrations of SFIB and sodium alginate were preferred for SFIB-MB (Table 1). The obtained SFIB-MB were subjected to different characterizations that assured the formation of smooth and spherical-shaped SFIB-MB, wherein NEV converted into the amorphous form. Based on FTIR interpretation, the changes in crystallinity of SFIB-MB were assured as an effect of solvent treatment on SFIB-containing protein structure. Finally, the release kinetics of SFIB-MB was documented to assure the effect of crystallinity changes in SFIB-MB on NEV release. In this section, the results and discussion of SFIB-MB were addressed in brief.

Fourier transform infrared spectrophotometry (FTIR)

Figure 1 depicts the FTIR spectra that show the different functionality present in each component of MB and the changes after the treatment. In brief, the FTIR spectra of NEV were observed at 3184.48 cm^{-1} (N-H bending primary amine), 3055.24 cm^{-1} (C-H bending alkene), 1639.49 cm^{-1} (C=C stretching alkenes), 1583.56 cm^{-1} (C=O stretching), 1159.22 cm^{-1} (C-N

bending amines) and 771.53 cm^{-1} (C-H bending), which confirmed the presence of NEV (Fig. 1a).[40,47] After that, the FTIR spectrum of isolated SFIB powder showed the peak for amide at 3280.92 cm^{-1}, which confirmed the presence of N-H bending. After that, amide I, II, and III stretchings were found at 1633.71 cm^{-1}, 1517.98 cm^{-1}, and 1236.37 cm^{-1} (C-N stretching), respectively (Fig. 1b).[11] The vibrational bands of sodium alginate were observed at 3257.77 cm^{-1} (O-H bending), 1597.06 cm^{-1} (C=O asymmetric stretching), 1406.11 cm^{-1} (C=O symmetric), and 1020.34 cm^{-1} (C-O-C stretching), which confirmed the presence of sodium alginate (Fig. 1c).[48] In the case of a physical mixture, a peak for 'amide I' at 1639.49 cm^{-1} and a peak for 'amide II' at 1587.42 cm^{-1} described the presence of NEV and SFIB with the absence of drug and polymer interaction (Fig. 1d). The FTIR spectrum of the blank formulation of MB depicts the peaks for 'amide I' at 1623.18 cm^{-1} and the peak for 'amide II' at 1520.67 cm^{-1} (Fig. 1e). In the case of the FTIR spectrum of the formulation, the main characteristic peak for amide I was found at 1600.92 cm^{-1}, whereas the peak for amide II was found obtained at 1501.38 cm^{-1} (Fig. 1f).

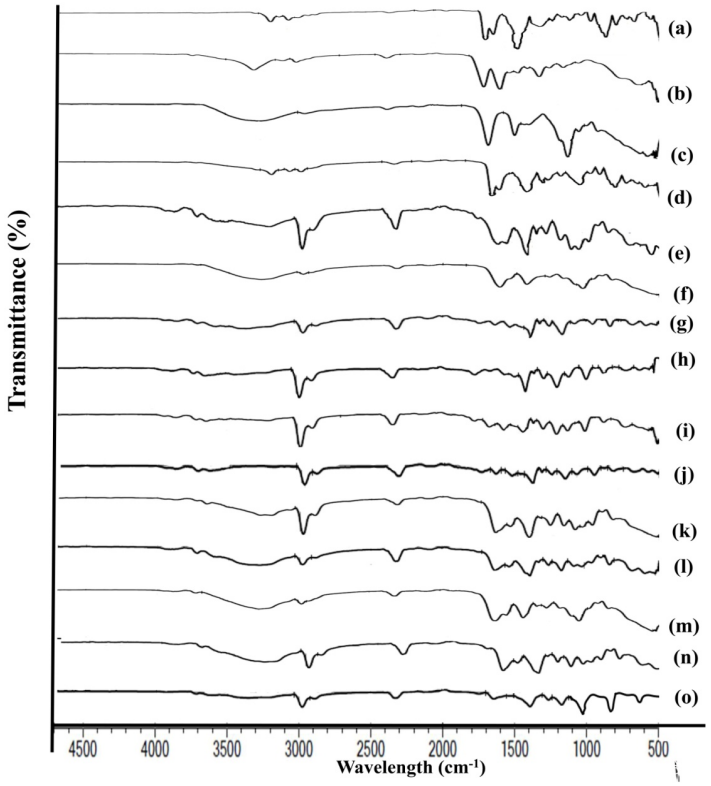

Figure 1: FTIR spectra of NEV (a), SFIB (b), sodium alginate (c), physical mixture (d), plain formulation (e), NEV-loaded SFIB-IPN-MB (f), ETH-2 (g), IPA-2 (h), ACT-2 (i), ETH-4 (j), IPA-4 (k), ACT-4 (l), ETH-6 (m), IPA-6 (n), and ACT-6 (o)

FTIR spectra of the ETH-2 batch showed the peak for amide I at 1622.57 cm^{-1}, whereas the peak for amide II was found at 1516.72 cm^{-1} (Fig. 1g). In the case of IPA-2 sample FTIR spectrum, the 'amide I' and 'amide II' principal peaks were obtained at 1618.49 cm^{-1}, and 1512.24 cm^{-1} (Fig. 1h). In the case of ACT (2 h), the FTIR spectra demonstrated peaks for 'amide I' and 'amide II' at 1633.71 cm^{-1}, and 1520.62 cm^{-1}, respectively (Fig. 1i).[38] The spectra of ETH-4, IPA-4, and ACT-4 h showed the characteristic bands of 'amide I' and 'amide II' at 1643.35 cm^{-1} and 1527.62 cm^{-1} (Fig. 1j), 1629.85 cm^{-1}, and 1527.62 cm^{-1} (Fig. 1k) and 1625.99 cm^{-1}, and 1514.67 cm^{-1} (Fig. 1l), respectively. In the case of the FTIR spectra of ETH-6, there are peaks observed for 'amide I' at 1628.42 cm^{-1} and 'amide II' at 1528.89 cm^{-1} (Fig. 1m). In the case of IPA-6, the peaks for 'amide I' and 'amide II' were found to be 1629.85 cm^{-1} and 1523.34 cm^{-1}, respectively (Fig. 1n), whereas the FTIR spectra of ACT-6 demonstrate the signals for 'amide I', and 'amide II' at 1635.64 cm^{-1} and 1521.78 cm^{-1}, respectively (Fig. 1o). Herein, changes were observed in peak intensity of the 'amide I' and 'amide II' bands, whereas there is a shift in FTIR wavelength after solvent treatment.

Possibly, these changes were found because of the alteration of 'α-helix' to 'β-sheet'. Herein, crystallinity changes were calculated based on the obtained FTIR of each SFIB-MB sample.

Calculation of the degree of crystallinity of NEV-loaded SFIB-MB

In this study, the obtained degree of crystallinity of NEV-loaded SFIB-IPN-MB was reported for each batch based on the values of vibrational bands. Table 2 depicts the crystallinity of NEV-loaded SFIB-IPN-MB after solvent (ETH, IPA, and ACT) treatment. Herein, the tangent baseline method shows the crystallinity of NEV-loaded SFIB-IPN-MB at about 0.81. In the case of ETH-2, the tangent baseline method shows the crystallinity of NEV-loaded SFIB-MB at about 0.88. In the case of IPA-2, the tangent baseline method shows the crystallinity of NEV-loaded SFIB-IPN-MB at about 0.87. In the case of ACT-2, the tangent baseline method provides the crystallinity of NEV-loaded SFIB-IPN-MB at about 0.87, respectively. After 6 h, the degree of crystallinity of ETH-6 was found to be 1.5, as confirmed by the tangent baseline method. In this case, the degree of crystallinity of IPA-6 was found to be 1.3, confirmed by the tangent baseline method. Meanwhile, the degree of crystallinity of ACT-6 was found to be 1.24 by the tangent baseline method. Hence, it assured the modification of crystallinity over time. Overall, the findings of the study reveal that the degree of crystallinity increases after treatment with different solvents over that in their initial stage. Importantly, it assured the changes in protein structure from amorphous 'α-helix' to crystalline 'β-sheet'.[38]

Table 2
ATR-FTIR values of wavenumber (cm^{-1}) for amide I and amide II and crystallinity calculation

Batch code	FTIR peak wavelength		Tangent baseline method
	Amide I peak (cm^{-1})	Amide II peak (cm^{-1})	
NEV-loaded SFIB-IPN-MB	1600	1501	0.81
ETH-2	1622	1516	0.88
IPA-2	1618	1512	0.87
ACT-2	1633	1520	0.87
ETH-4	1643	1527	1.18
IPA-4	1629	1527	1.18
ACT-4	1625	1514	1.14
ETH-6	1628	1528	1.5
IPA-6	1629	1523	1.3
ACT-6	1635	1521	1.24

Ethanol (ETH); isopropyl alcohol (IPA); and acetone (ACT)

Differential scanning calorimetry (DSC)

Figure 2 presents the thermal changes in samples. In brief, the thermogram of NEV showed a sharp endothermic peak at 245.64 °C, which assured the crystalline form of NEV.[47] The thermogram of SFIB exhibited broad endothermic transitions at 273.71 °C, which confirms the extracted material was amorphous SFIB.[11] Then, the thermogram of NEV-loaded SFIB-IPN-MB displayed endothermic conversions at 216.33 °C, 245.36 °C and 274.73 °C, demonstrating compatibility amongst sodium alginate, NEV, and SFIB, respectively. Moreover, it indicates the decrease in the crystallinity of NEV in the thermogram of NEV-loaded SFIB-IPN-MB, compared to that of plain NEV, which assured the maximum conversion of NEV into an amorphous form.

Powder X-ray diffraction studies (PXRD)

Figure 3 depicts the behavior of solids in terms of crystalline and amorphous. In brief, the diffractogram of NEV exposed sharp and high-intensity points at 2θ values of 9.382°, 13.183°, 19.164°, 25.675° and 33.010°, which assured NEV existed in a highly crystalline form (Fig. 3a). In the diffractogram of SFIB, the maximum low-intensity points were detected (Fig. 3b). Primarily, deflection peaks were obtained at 2θ values of 12.67°, 20.42°, 24.57°, 27.83°, and 37.25°. No high-intensity graph in the diffractogram indicates the less crystalline and

highly amorphous nature of SFIB.[44] In the case of NEV-loaded SFIB-IPN-MB, 2θ values originated at 13.80°, 21.22°, 27.02°, 36.18°, and 42.50°, revealing the presence of NEV and SFIB in the formulation (Fig. 3c). Besides, the low intensity peak validated that the nature of the drug changes from crystalline to amorphous nature. Possibly, it is because of the interaction of drugs with SFIB and forces involved in SFIB and sodium alginate.

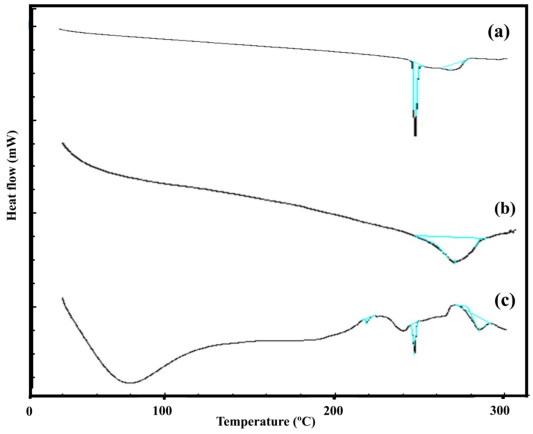

Figure 2: Thermograms of (a) NEV, (b) SFIB, and (c) NEV-loaded SFIB-IPN-MB

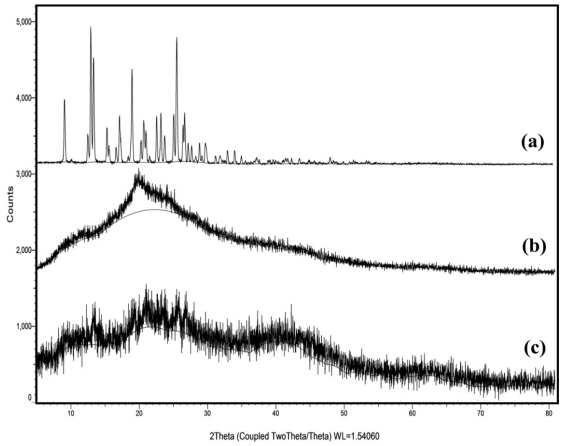

Figure 3: Diffractograms of (a) NEV, (b) SFIB, and (c) NEV-loaded SFIB-IPN-MB

Scanning electron microscopy (SEM)

Figure 4 depicts the surface morphology of NEV-loaded SFIB-IPN-MB. In brief, NEV-loaded SFIB-IPN-MB was demonstrated to be spherical, with a rough and porous external surface. It assured the absence of surface defects, such as irregular shape, tailing effect, a small fraction of floating microbeads, *etc*. The porous surface of NEV-loaded SFIB-IPN-MB will be beneficial for the incorporation of dissolution media that can help modify the NEV release. In addition, the spongy nature of NEV-loaded SFIB-IPN-MB assists in its floating on the surface of dissolution media, as well as for penetration of dissolution media, followed by drug release.

Percentage entrapment efficiency and drug content

Entrapment efficacy refers to the overall amount of drug entrapped in the carrier. Herein, the entrapment of NEV in the prepared NEV-loaded SFIB-IPN-MB was found to be 56.33%, 57.82%, and 61.71% for batches B_3, B_4, and B_5, respectively (n = 3). Thus, batch B_5 exhibits a higher entrapment efficiency than batches B_3 and B_4. For NEV-loaded SFIB-IPN-MB, the percent DC was found to be 68.74%, 72.53%, and 80.40% for batches B_3, B_4, and B_5, respectively (n = 3). Herein, batch B_5 resulted in better content uniformity than B_3 and B_4.

Micromeritic properties

The average diameter of the freshly prepared optimized batch (B_5) was found to be 1.273 µm. The tapped density and bulk density of B_5 was found to be 0.90 g/mL and 0.87 g/mL, accordingly. Importantly, the overall density of NEV-loaded SFIB-IPN-MB is less than the density of stomach fluid (1.4 g/cc). Hence, it is beneficial for floating of NEV-loaded SFIB-MB on the surface of the stomach dissolution fluid. Carr's index was found to be 3.33%, which indicates the excellent flow property of floating MB. The angle of repose of batch B_5 was found to be 16.98°, which confirmed the excellent flow of NEV-loaded SFIB-IPN-MB. Overall, the designed NEV-loaded SFIB-IPN-MB shows an excellent flow property that can help to fill the capsule with uniform weight.

Floating profile of NEV-loaded SFIB-IPN-MB

For excellent floating behavior, there is a need to validate the FLT, TFT and % buoyancy. Herein, the benefits of low-density SFIB demonstrate good floating behavior in stomach fluid (pH = 1.5 HCl buffer). The optimized NEV-loaded SFIB-IPN-MB shows an FLT of 10-15 seconds only, whereas the TFT of NEV-loaded SFIB-IPN-MB was found to be more than 12 hours. The % buoyancy of NEV-loaded SFIB-IPN-MB was obtained to be 96.80% (w/w). Herein, the low density of SFIB resulted in the

low-density NEV-loaded SFIB-IPN-MB, which displayed outstanding floating performance.

Overall, the designed NEV-loaded SFIB-IPN-MB complies with the good floating profile for FDDS.

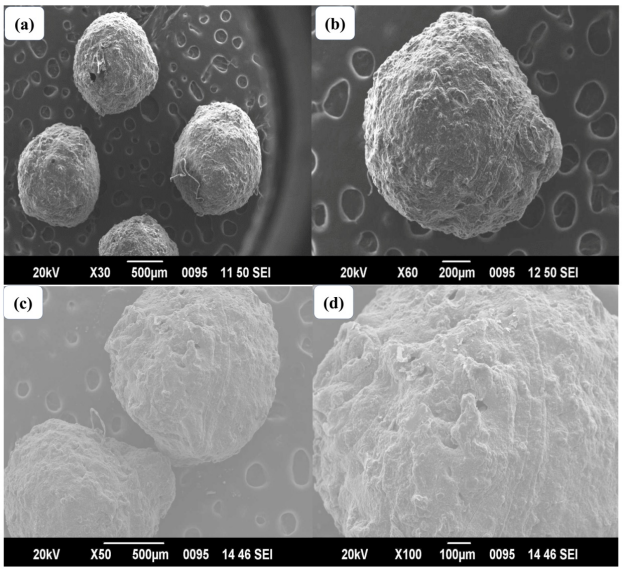

Figure 4: SEM images of NEV-loaded SFIB-IPN-MB

Table 3
Process parameters of micromeritic properties

Batch code	Average particle size (mm)	BD (g/mL)	TD (g/mL)	Compressibility index (%)	Angle of repose (2θ Degree)	Significance of flow property
B_1	1.082	1.04	1.08	3.703	24.49	Excellent
B_2	1.138	0.98	1.04	5.76	19.66	Excellent
B_3	0.981	0.98	1.02	3.921	27.92	Good
B_4	1.129	0.92	0.98	6.122	17.28	Excellent
B_5	1.273	0.87	0.90	3.33	16.98	Excellent

***In-vitro* dissolution study**

It is worth mentioning that the amount of 'β-sheet' present in SFIB provides the crystalline behavior to SFIB-based NEV-loaded SFIB-IPN-MB. In this, the crystalline nature of NEV-loaded SFIB-IPN-MB gives the mechanical barrier to drug release from the dosage form. In the current work, the crystallinity modification gives additional benefits to the sustained release of a NEV from floating NEV-loaded SFIB-IPN-MB. In brief, the release of NEV from NEV-loaded SFIB-IPN-MB was found to be 65.132% in 12 hours. It follows the Higuchi matrix release kinetics (r^2 = 0.9969, k = 3.0), whereas the 'n' value was found to be 0.4684, which confirmed the non-Fiction diffusion as a drug transport mechanism. After the treatment with different solvents (ETH, IPA, and ACT), changes in the degree of crystallinity were found. After treatment of 2 hours, batch ETH-2 shows 38.160% of NEV release from NEV-loaded SFIB-IPN-MB. It follows the Korsmeyer Peppas as a release kinetics model (r^2 = 0.9821), wherein it shows Fickian diffusion as a drug transport mechanism (n = 0.3781, k = 3.2615). In the case of batch IPA-2, it demonstrates 34.025% of NEV release from NEV-loaded SFIB-IPN-MB. As well, it follows the Korsmeyer Peppas as a release kinetics model (r^2 = 0.9733), wherein it illustrates Fickian diffusion as a drug transport mechanism (n = 0.3686, k = 3.2667). In the case of batch ACT-2, it confirmed 34.709% of NEV release from NEV-loaded SFIB-IPN-MB. Then, it follows the Korsmeyer Peppas as a release kinetics model (r^2 = 0.9922), wherein it gives an idea about Fickian diffusion as a drug transport mechanism (n = 0.3363, k = 4.0706). Here, the suppression of drug release was obtained, in contrast to the non-

treated NEV-loaded SFIB-IPN-MB, as a result of the alteration in crystallinity of NEV-loaded SFIB-IPN-MB due to solvent treatment. Surprisingly, the ETH-6 batch of NEV-loaded SFIB-IPN-MB shows a 25.853% release in 12 hours. It follows the first-order release kinetics (r^2 = 0.9777, k = 0.1700), whereas the 'n' value was found to be 0.7478, assuring non-Fickian diffusion as a drug transport mechanism from floating beads. Herein, changes in drug release kinetics were obtained over the non-treated floating beads because of the significant changes in the degree of crystallinity of NEV-loaded SFIB-IPN-MB (ETH-6) at the end of 6 hours. The case of IPA-6 and ACT-6 shows 27.447% and 27.844% drug release, and Fickian diffusion as a drug transport mechanism (n = 0.4588 and 0.4227). In addition, both formulations show the Korsmeyer Peppas as a best-fit release kinetics model. This work confirmed that the time required for solvent treatment is an important parameter that results in the modulation of the degree of crystallinity and an impact on drug release from floating MB. Importantly, the optimized batch ETH-6 shows the sustained release of NEV from floating beads. In addition, the present work confirmed that the changes in the crystallinity of SFIB due to the conversion of 'α-helix' to 'β-sheet' after solvent treatment assist to delay the drug release from the formulation. Similarly, the dissolution studies of different batches demonstrate a changed quantity of drug release depending on the crystallinity of SFIB. Hence, it reveals that the crystallinity of the SFIB polymer matrix is the control point for the dissolution profile of SFIB protein.[38] Figure 5 presents the *in-vitro* release profile of floating NEV-loaded SFIB-IPN-MB.

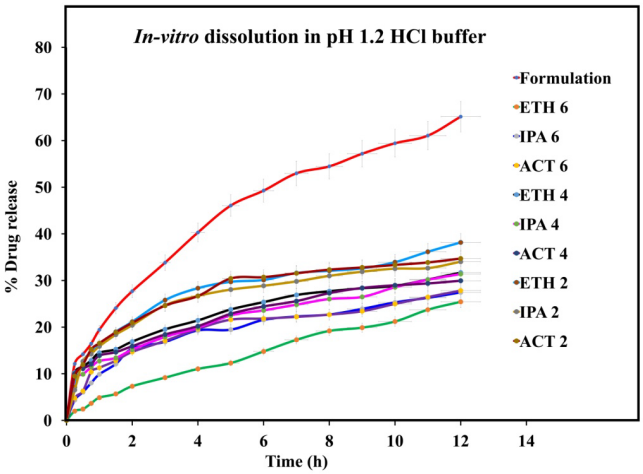

Figure 5: Presentation *of in-vitro* release profile of floating NEV-loaded SFIB-IPN-MB

Table 4
In-vitro drug release kinetic models, regression output and best-fit model

Parameters / Batch	Zero (r^2)	First (r^2)	Matrix (r^2)	Peppas (r^2)	Hix. Crow. (r^2)	'n' value	'k' value	Best fit model	Drug release (12 h)
Formulation	0.8328	0.9479	0.9969	0.9962	0.9190	0.4684	3.0091	Matrix	65.132
ETH-6	0.9777	0.9857	0.9572	0.8584	0.9834	0.7478	0.1700	1st order	25.430
IPA-6	0.7207	0.7912	0.9817	0.9886	0.7696	0.4588	1.4174	Peppas	27.447
ACT-6	0.6386	0.7304	0.9690	0.9822	0.7026	0.4227	1.7833	Peppas	27.844
ETH-4	0.4133	0.6227	0.9408	0.9953	0.5659	0.3058	4.1144	Peppas	31.691
IPA-4	0.6338	0.7564	0.9710	0.9934	0.7207	0.3405	3.1651	Peppas	31.394
ACT-4	0.4793	0.6558	0.9485	0.9922	0.6064	0.3105	3.8648	Peppas	29.946
ETH-2	0.4832	0.6703	0.9471	0.9821	0.6183	0.3781	3.2615	Peppas	38.160
IPA-2	0.3489	0.5762	0.9301	0.9733	0.5157	0.3686	3.2667	Peppas	34.025
ACT-2	0.2714	0.5526	0.9247	0.9922	0.4829	0.3363	4.0706	Peppas	34.709

Ethanol (ETH); Isopropyl alcohol (IPA); Acetone(ACT); Release exponent (n); Release rate constant (k), and Regression factor (r^2)

Table 4 displays the release kinetics of floating NEV-loaded SFIB-IPN-MB. The statistical method was performed to ensure the difference in the dissolution profile of the formulation and ETH-6 batch. In this case, the log *p*-value was found to be less than 0.0001 (95% confidence interval), which indicates the significant difference between the non-treated formulation and optimized ETH-6 batch. Moreover, the F_1 and F_2 were obtained to be 54 ($F_1 > 15$) and 44 ($F_2 < 50$), respectively, which reveals the difference in the dissolution profile of the non-treated formulation and optimized ETH-6 batch.

CONCLUSION

The present work presents successful efforts to formulate floating and crystallinity-tuned MB using SFIB and sodium alginate for delivery of NEV. To the best of our knowledge, no report is available on the development of crystallinity-adjusted floating microbeads. In brief, the isolation and utilization of SFIB protein were accomplished from silk industry waste cocoons, which can boost the valorization of waste for pharmaceutical applications. This obtained SFIB exhibited the potential for good floating behavior due to its low density, compared to that of stomach fluid (1.4 g/mL). The micromeritics of the designed NEV-loaded SFIB-IPN-MB revealed a good flow property. Moreover, non-treated NEV-loaded SFIB-IPN-MB shows spherical and smooth surface morphology, whereas it resulted in 65.13% drug release in 12 hours, following the Higuchi matrix release kinetics. Interestingly, the thermogram and diffractogram of NEV demonstrate the conversion into a less crystalline form due to the effect of the polymer matrix in the optimized batch. In addition, the optimized floating MBs resulted in a good floating profile, including FLT, TFT, and % buoyancy. As well, the solvent annealing to the designed NEV-loaded MB resulted in significant changes in the crystallinity of NEV-loaded SFIB-IPN-MB with time, which were confirmed by using FTIR-based methods, namely the tangent baseline method. Herein, the FTIR study revealed shifting wave numbers, as well as the peak intensity of amide I and amide II bonds present in SFIB-based floating MB. Importantly, changes in crystallinity are possible due to the changes in SFIB amorphous 'α-helix' to the crystalline 'β-sheet'. As a response, the crystalline nature of SFIB retards the release of NEV from NEV-loaded IPN-MB up to 25.43% (12 hours), as compared to non-treated formulation ($\log p < 0.0001$). The release kinetics confirmed the shift in release kinetics from the Higuchi matrix to 1st order release kinetics, along with non-Fickian diffusion as a drug transport mechanism from floating MB. The 'F_1' and 'F_2' analyses validated the difference in the dissolution profile of the non-treated formulation and optimized ETH-6 batch. In conclusion, crystallinity-modified floating NEV-loaded SFIB-IPN-MB can be used for sustained release of BCS class-II drug. In the future, the present strategy can be preferred to tune the drug release from a selected protein carrier.

ACKNOWLEDGMENT: The authors are thankful to the Management and Principal of H. R. Patel Institute of Pharmaceutical Education and Research, Shirpur, for providing the required facility to conduct the present work smoothly.

REFERENCES

[1] V. Iannuccelli, G. Coppi, M. T. Bernabei and R. Cameroni, *Int. J. Pharm*., **174**, 47 (1998), https://doi.org/10.1016/S0378-5173(98)00229-4

[2] P. Shrivastava, S. Vyas, R. Sharma, N. Mody, L. Gautam, *et al*., in "Nanoengineered Biomaterials for Advanced Drug Delivery", edited by M. Mozafari, Elsevier, USA, 2020, pp. 473-498, https://doi.org/10.1016/B978-0-08-102985-5.00020-6

[3] B. Choi, H. J. Park, S. Hwang and J. Park, *Int. J. Pharm*., **239**, 81 (2002), https://doi.org/10.1016/s0378-5173(02)00054-6

[4] S. P. Poornima and S. Priya, *Indian J. Pharm. Educ. Res*., **55**, s100 (2021), https://doi.org/10.5530/ijper.55.1s.41

[5] J. Tripathi, P. Thapa, R. Maharjan and S. H. Jeong, *Pharmaceutics*, **11**, 193 (2019), https://doi.org/10.3390/pharmaceutics11040193

[6] B. Nanjwade, S. Adichwal and K. Sutar, *J. Drug. Deliv. Sci. Technol*., **22**, 327 (2012), https://doi.org/10.1016/S1773-2247(12)50055-9

[7] R. Shakya, P. Thapa and R. N. Saha, *Asian J. Pharm. Sci*., **8**, 191 (2013), https://doi.org/10.1016/j.ajps.2013.07.025

[8] H. Patil, R. V. Tiwari and M. A. Repka, *J. Drug. Deliv. Sci. Technol*., **31**, 65 (2016), https://doi.org/10.1016/j.jddst.2015.12.002

[9] S. Baumgartner, J. Kristl, F. Vrečer, P. Vodopivec and B. Zorko, *Int. J. Pharm*., **195**, 125 (2000), https://doi.org/ 10.1016/s0378-5173(99)00378-6

[10] A. J. Moës, *Crit. Rev. Ther. Drug. Carrier Syst*., **10**, 143 (1993), https://pubmed.ncbi.nlm.nih.gov/8370085

[11] S. Nangare, S. Dugam, P. Patil, R. Tade and N. Jadhav, *Nanotechnology*, **32**, 035101 (2020), https://doi.org/ 10.1088/1361-6528/abb8a9

[12] P. Rathod, H. More, S. Dugam, P. Velapure and N. Jadhav, *J. Pharm. Innov.*, **16**, 226 (2021), https://doi.org/ 10.1007/s12247-020-09440-6
[13] A. Deshpande, C. Rhodes, N. Shah and A. Malick, *Drug Dev. Ind. Pharm.*, **22**, 531 (1996), https://doi.org/10.3390/molecules26195905
[14] S.-J. Hwang, H. Park and K. Park, *Crit. Rev. Ther. Drug. Carrier Syst.*, **15**, 243 (1998), https://doi.org/10.1615/critrevtherdrugcarriersyst.v28.i1.20
[15] T. O. Ajala, O. T. Moshood and O. A. Odeku, *Br. J. Pharmacol.*, **6**, 1 (2021), https://doi.org/10.5920/bjpharm.854
[16] H. Roy, S. Balaiah and T. V. Kumar, *Res. J. Pharm. Technol.*, **11**, 2276 (2018), https://doi.org/10.5958/0974-360X.2018.00422.5
[17] A. Kumar, K. Mahalakshmi and M. Rao, *Int. J. Life Sci. Rev.*, **1**, 137 (2015), https://doi.org/10.13040/IJPSR.0975-8232
[18] S. K. Mishra and K. Pathak, *Acta Pharm.*, **58**, 187 (2008), https://doi.org/10.2478/v10007-008-0001-8
[19] A. Okunlola, O. A. Odeku and R. P. Patel, *J. Excip. Food Chem.*, **3**, 17 (2012), https://ojs.abo.fi/ojs/index.php/jefc/article/view/143
[20] I. U. Khan, M. Shoukat, M. Asif, S. H. Khalid, S. Asghar *et al.*, *Microorganisms*, **10**, 1171 (2022), https://doi.org/10.3390/microorganisms10061171
[21] S. S. Gupta, G. Sahu, M. Sharma, S. Chandrakar, V. D. Sahu *et al.*, *Res. J. Pharm. Tech.*, **7**, 848 (2016), https://doi.org/10.5958/0974-360X.2016.00160.8
[22] N. J. Vickers, *Curr. Biol.*, **27**, R713 (2017), https://doi.org/10.1016/j.cub.2017.05.064
[23] S. Abdeen, R. R. Isaac, S. Geo, S. Sornalekshmi, A. Rose *et al.*, *Nano. Biomed. Eng.*, **5**, 39 (2013), https://doi.org/10.5101/nbe.v5i1
[24] S. N. Nangare and P. O. Patil, *Nano. Biomed. Eng.*, **12**, 281 (2020), https://doi.org/10.5101/nbe.v12i4
[25] T. Imsombut, Y. Srisuwan, P. Srihanam and Y. Baimark, *Powder Technol.*, **203**, 603 (2010), https://doi.org/10.1016/j.powtec.2010.06.027
[26] S. Faragò, G. Lucconi, S. Perteghella, B. Vigani, G. Tripodo *et al.*, *Pharm. Dev. Technol.*, **21**, 453 (2016), https://doi.org/10.3109/10837450.2015.1022784
[27] Y. Qi, H. Wang, K. Wei, Y. Yang, R.-Y. Zheng *et al.*, *Int. J. Mol. Sci.*, **18**, 237 (2017), https://doi.org/10.3390/ijms18030237
[28] C. Pignatelli, G. Perotto, M. Nardini, R. Cancedda, M. Mastrogiacomo *et al.*, *Acta Biomater.*, **73**, 365 (2018), https://doi.org/10.1016/j.actbio.2018.04.025
[29] M. Ichikawa, S. Watanabe and Y. Miyake, *J. Pharm. Sci.*, **80**, 1062 (1991), https://doi.org/10.1002/jps.2600801113
[30] A. Badwan, A. Abumalooh, E. Sallam, A. Abukalaf and O. Jawan, *Drug Dev. Ind. Pharm.*, **11**, 239 (1985), https://doi.org/10.3109/03639048509056869
[31] S. Shiraishi, T. Imai and M. Otagiri, *Biol. Pharm. Bull.*, **16**, 1164 (1993), https://doi.org/10.1248/bpb.16.1164
[32] Y. Murata, K. Kofuji and S. Kawashima, *J. Biomater. Sci. Polym. Ed.*, **14**, 581 (2003), https://doi.org/10.1163/15685620360674263
[33] Y. Murata, N. Sasaki, E. Miyamoto and S. Kawashima, *Eur. J. Pharm. Biopharm.*, **50**, 221 (2000), https://doi.org/10.1016/s0939-6411(00)00110-7
[34] F. Stops, J. T. Fell, J. H. Collett, L. G. Martini, H. L. Sharma *et al.*, *Int. J. Pharm.*, **308**, 14 (2006), https://doi.org/10.1016/j.ijpharm.2005.09.039
[35] K. Sowjanya, K. Shoba Deepthi and A. Bharathi, *Int. J. Pharm. Pharm. Sci.*, **4**, 368 (2012), https://innovareacademics.in/journal/ijpps/Vol4Suppl5/5094.pdf
[36] T. E. Manyarara, S. Khoza, A. Dube and C. C. Maponga, *MRS Adv.*, **3**, 2203 (2018), https://doi.org/10.1557/adv.2018.320
[37] S. Macha, C. L. Yong, T. R. MacGregor, M. Castles, A. M. Quinson *et al.*, *J. Clin. Pharmacol.*, **49**, 1417 (2009), https://doi.org/10.1177/0091270009344856
[38] S. Dugam, S. Nangare, A. Gore, S. Wairkar, P. Patil *et al.*, *Int. J. Polym. Mater. Polym. Biomater.*, 1 (2021), https://doi.org/10.1080/00914037.2021.1981318
[39] D. N. Rockwood, R. C. Preda, T. Yücel, X. Wang, M. L. Lovett *et al.*, *Nat. Protoc.*, **6**, 1612 (2011), https://doi.org/10.1038/nprot.2011.379
[40] B. V. Hari, A. B. Reddy and B. S. Rani, *J. Young. Pharm.*, **2**, 350 (2010), https://doi.org/10.4103/0975-1483.71622
[41] X. Hu, D. Kaplan and P. Cebe, *Macromolecules*, **39**, 6161 (2006), https://doi.org/10.1021/ma0610109
[42] S. Nangare and P. Patil, *Anal. Chim. Acta*, **1271**, 341474 (2023), https://doi.org/10.1016/j.aca.2023.341474
[43] R. Dhole, U. Patil and N. Jadhav, *J. Res. Pharm.*, **23**, 997 (2019), https://doi.org/10.35333/jrp.2019.64
[44] J. Pantwalawalkar and S. Nangare, *Ind. J. Pharm. Edu. Res.*, **56**, 396 (2022), https://doi.org/10.5530/ijper.56.2.59
[45] N. R. Jadhav, H. R. Bhakare and B. K. Bhawale, *Asian J. Pharm.*, **6**, 44 (2012), https://doi.org/10.22377/ajp.v6i1.72
[46] F. P. Flores and F. Kong, *Annu. Rev. Food Sci. Technol.*, **8**, 237 (2017), https://doi.org/10.1146/annurev-food-030216-025720
[47] S. Mehta and N. Jindal, *AAPS Pharm. Sci. Tech.*, **16**, 67 (2015), https://doi.org/10.1208/s12249-014-0183-y
[48] N. Gupta and N. Aggarwal, *AAPS Pharmscitech.*, **8**, E143 (2007), https://doi.org/10.1208/pt0802048